PNAS RESEARCH ARTICLE | APPLIED PHYSICAL SCIENCES

A hovering bubble with a spontaneous horizontal oscillation

Man Hu[a], Yuqi Li[a], Li Chen[a], Wenna Wu[a], Peng Huo[a], Xi Gu[a], Feng Wang[b,1], and Daosheng Deng[a,1]

Edited by David Weitz, Harvard University, Cambridge, MA; received July 10, 2024; accepted September 24, 2024

Active matters, characterized by multi-mode motions, have been emerging for both engineering and biological applications. Generally, active objects rely on the symmetry-broken structures, compositions, or interfacial activities through a physical or chemical approach. Here, we report an active bubble spontaneously hovering with a horizontal oscillation at the solid/liquid interface by impacting a stationary laser beam into a liquid through a transparent solid cover. This spontaneous oscillation mode of the bubble synchronizes with that of the interfacial temperature and hydrodynamical flow. A physical mechanism is proposed, and the scaling analysis of the oscillation frequency agrees well with experiments in various liquids under different laser powers. Additionally, the bubble trajectory rotates azimuthally, arising from the symmetry breaking of the vortex pair accompanying the oscillation. Moreover, the double pendulum of oscillation bubbles has been demonstrated, achieving a preferable oscillation direction in a controllable way. These findings would not only advance our understanding of active matters but also shed light on the bubble-mediated technological applications, such as microrobots and drug deliveries.

bubble oscillation | Marangoni flow | stagnation flow | near-infrared laser

Significance

Active matters have been emerging for the micro/nanorobots and biological applications, and rely on the symmetry-broken structures, compositions, or interfacial activities through a physical or chemical approach. Here, we report an active bubble spontaneously hovering with a horizontal oscillation at the solid/liquid interface by impacting a stationary laser beam into a liquid. Also the bubble trajectory is rotating azimuthally within a long period, arising from the symmetry breaking of the vortex pair accompanying this oscillation. Moreover, the double pendulum of oscillation bubbles has been demonstrated, achieving a preferable oscillation direction in a controllable way. These findings would not only advance our understanding of active matters but also shed light on the bubble-mediated technological applications.

Active tiny objects, such as self-propelled Brownian particles or microswimmers, which are capable of consuming energy from their environment and converting it into kinetic energy for the subsequent directional motion or the desirable navigation, have provided insight into the micro/nanorobots for engineering and biological applications (1–6). In order to mimic the natural system to decipher their complicated dynamics and reveal physical principles, the artificial objects have been designed sophisticatedly by exploiting the symmetry-broken structures, such as disks, rods, or particles, to promote chemical gradients or favorable activity in the medium (7–10). For example, Polydimethylsiloxane (PDMS) disks with asymmetric surface patterns, or striped nanorods consisting of different segments, are propelled by the impulse of bubbles generated by the platinum-catalyzed decomposition of hydrogen peroxide (11, 12). Janus particles rely on different interfacial compositions to convert uniformly distributed sources of energy into the net motion (13, 14).

Besides constructing asymmetric particles, another strategy to drive the active droplets or bubbles is utilizing symmetry-broken interfacial activities physically (such as temperature gradient to form the thermal Marangoni effect) or chemically (such as concentration gradient to cause the solutal Marangoni effect) (15–20). Specifically, since the surface tension of liquids can be efficiently tuned optically due to the photothermal effect, the laser-driven thermal Marangoni convection has been extensively investigated to generate the self-propelled or self-guided motion of the objects at the microscopic scale (21–26). Intriguingly, the periodic bouncing of a plasmonic bubble in a binary liquid has been identified due to the competition between the disturbing solutal Marangoni force and the restoring thermal Marangoni force (27). Also, the periodic bouncing of a photothermal bubble in a pure liquid medium has been demonstrated arises from the thermal Marangoni force within the temperature inversion layer (28).

However, this motion mode for those bubbles in either a pure or multi-component liquid is typically constrained along the laser incident direction, consequently imposing an inherent limitation for the versatile manipulation and the relevant applications. Hence, it would be intriguing to explore the multi-mode motion by breaking the azimuthal or radial symmetry of either the morphology of the objects or their trajectories. Indeed, in oil-on-water droplets, the oil droplets become polygons with distinct edges and corners, since the solutal Marangoni effect due to the evaporation of oil produces a strong flow sufficient to overcome the spherical shape of the droplet (29).

In this work, by impacting a stationary near-infrared laser beam vertically onto a liquid through a transparent solid cover, we observe the spontaneous symmetry-breaking behaviors of an active photothermal bubble, which exhibits a remarkable horizontal oscillation hovering at the liquid/solid interface. This oscillation mode of the bubble is

Author affiliations: [a]Department of Aeronautics and Astronautics, Fudan University, Shanghai 200433, China; and [b]Center for Combustion Energy, Department of Energy and Power Engineering, Tsinghua University, Beijing 100084, China

Author contributions: M.H. and D.D. designed research; M.H. and F.W. performed research; M.H., Y.L., L.C., W.W., P.H., X.G., F.W., and D.D. analyzed data; and M.H., F.W., and D.D. wrote the paper.

The authors declare no competing interest.

This article is a PNAS Direct Submission.

[1]To whom correspondence may be addressed. Email: fengwang2023@tsinghua.edu.cn or dsdeng@fudan.edu.cn.

This article contains supporting information online at https://www.pnas.org/lookup/suppl/doi:10.1073/pnas.2413880121/-/DCSupplemental.

Published October 24, 2024.

synchronizing with that of the interfacial temperature and hydrodynamical flow, in a fashion to be controlled by an external stationary laser beam. A physical mechanism is proposed by taking into account the synergistic effect of the driven drag force arising from the stagnation flow and the restoring thermal Marangoni force. The scaling analysis of the oscillation frequency agrees well with the experiments in various liquids under different laser powers. Additionally, the rotation of the bubble trajectory is explained by the asymmetry of the vortices associated with the oscillation. Moreover, the double pendulum of oscillation bubbles has been demonstrated, achieving a preferable oscillation direction in a controllable way along the centerline of the laser beams. These findings will not only advance our understanding of active matters but also shed light on the bubble-mediated technological applications, such as microrobots and drug deliveries.

Results

Observation of the Horizontal-Oscillation Bubble. A 980-nm near-infrared laser with a beam size $2r_l = 1$ mm impacts upon ethanol, after passing through a 250-μm-thick sapphire glass (optically transparent at 185 to 5,000 nm) (Fig. 1*A*). Arising from the volumetric absorption of photon energy [which has an absorption coefficient about 7.3/m at 980 nm wavelength for ethanol (30)], once the laser power exceeds the threshold value $P \approx 12$ W corresponding to the averaged laser intensity $I_l \approx 1.5 \times 10^3$ W/cm^2, a photothermal bubble is formed within the liquid (Fig. 1*A*, detail of the experimental setup is shown in *SI Appendix*, Fig. S1). As the bubble grows and expands under the illumination of the stationary laser, its diameter (d) increases with time (31), and the bubble is expected to be floating at the liquid–solid interface at a large diameter [$d > d_{up}$ (Fig. 1*B*)].

However, within a certain diameter window ($d_{low} < d < d_{up}$), a remarkable spontaneous symmetry-breaking motion is observed, i.e., a horizontal-oscillation motion confined within the xy-plane at the liquid–solid interface (Fig. 1*B*). This horizontal oscillation of bubble within one typical period (6.03 s $< t <$ 6.071 s) is demonstrated by high-speed images from the *Top–Down* view (Fig. 1*C* and Movie S1) without displacement along the vertical direction from the side view (Movie S2). This horizontal oscillation of the photothermal bubble is sustainable and can endure for tens of seconds, as indicated by the oscillation of the bubble center (x, y) in Fig. 1*B*.

By zooming in the spatiotemporal evolution of bubble center position (x, y) within 0.5 s (Fig. 1*D*), the probability density function (PDF) of the oscillation frequency is calculated with a peak frequency of about 24 Hz (Fig. 1*E*). Additionally, the trajectory of the oscillation bubble within 3 s (Fig. 1*F*) illustrates the rotation of the oscillation direction, and the associated phase portraits (Fig. 1*G*) indicate an instantaneous acceleration process within a very small displacement ($s < 0.05$ mm), where the amplitude of the velocity increases with the displacement.

Oscillation Synchronizing with Temperature. To further characterize this photothermal bubble produced by laser impacting on ethanol, the relevant spatiotemporal evolution of temperature is directly visualized by thermal images (Fig. 2*A* and Movie S3). Accompanying the bubble oscillation, the warm or hot region with a high temperature moves backward and forward along the oscillation axis. By plotting the temperature distribution along the oscillation axis (the solid line in Fig. 2*A*) into a spatial-temporal colormap (Fig. 2*B*), the periodic motion of temperature distribution becomes straightforward.

More quantitatively, at given characteristic positions (such as *A, O, B* for $\xi = -0.15, 0, 0.25$ mm), the temperature evolution

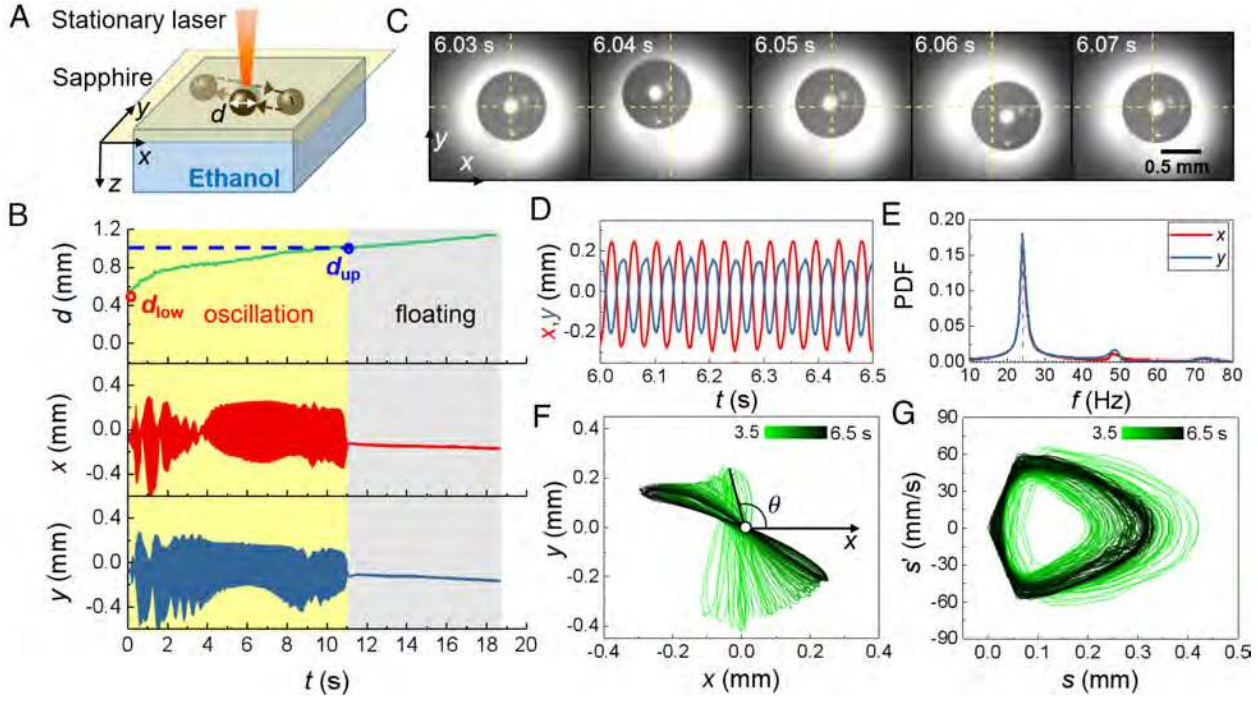

Fig. 1. Spontaneous horizontal oscillation of an active photothermal bubble. (*A*) Schematic of the oscillating photothermal bubble during a stationary laser impacting on ethanol through a transparent cover glass. (*B*) Time-dependent bubble diameter d, center position x and y (the bubble becoming visible at $t = 0$ s) at the laser power $P = 21$ W. (*C*) High-speed images for the oscillating bubble within one typical period (6.03 s $< t <$ 6.071 s) from *Top–Down* view ($x - y$ plane). (*D*) Zoom-in bubble center (x, y) versus time clearly demonstrating the periodic oscillation. (*E*) PDF of bubble oscillation frequencies with $f = 24$ Hz at the peak. (*F*) Oscillation trajectory of the bubble center in the $x - y$ plane within 3 s, and the trajectory angle θ defined by the angle between the bubble oscillation axis and the x-axis. (*G*) The phase portraits of the bubble oscillation corresponding to the motion in (*F*).

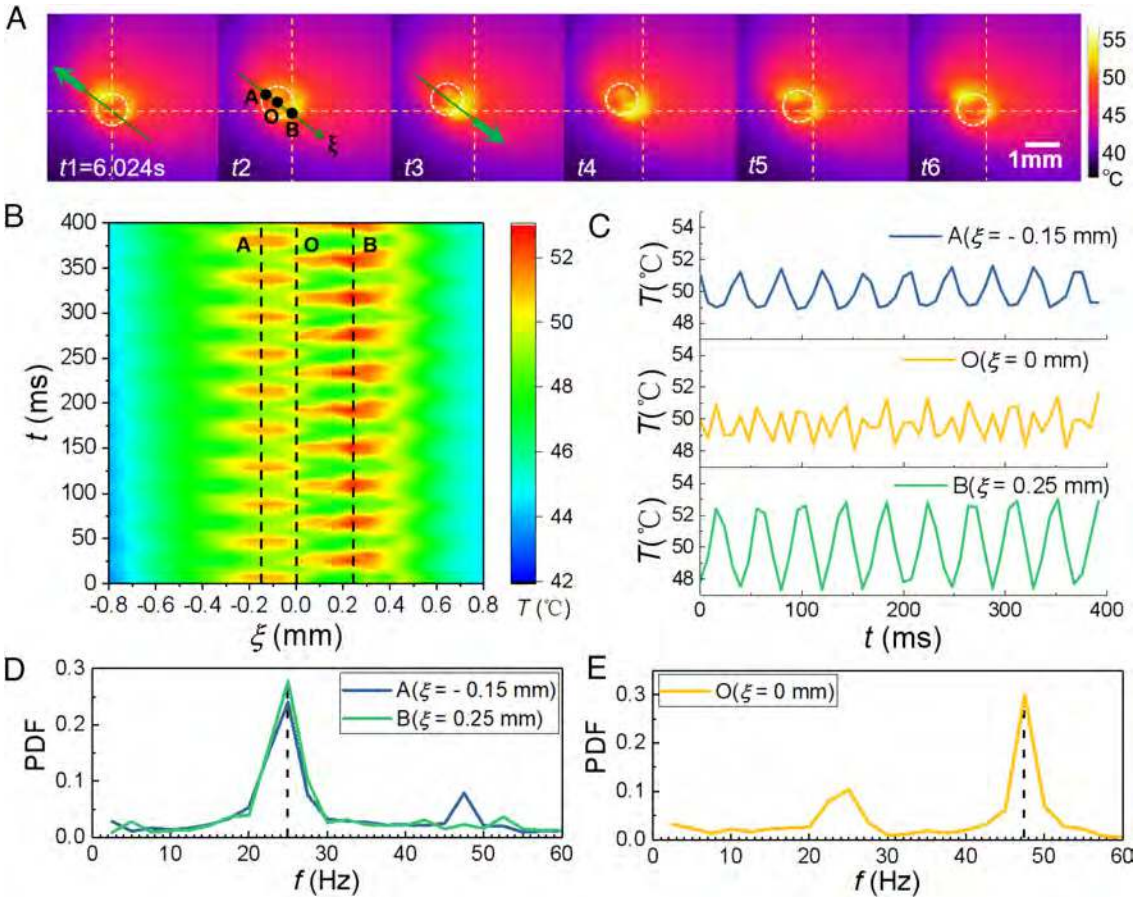

Fig. 2. Spatiotemporal evolution of temperature distribution synchronizing with bubble oscillation in ethanol. (*A*) *Top–Down* view of thermal images for bubble oscillating within one typical period at $P = 21$ W (the interval is 8 ms between snapshots from *t*1 to *t*6). The white circles, green lines, and green arrows for the bubble position, oscillation axis, and moving direction, respectively. (*B*) Temperature evolution along the bubble oscillation axis during 400 ms, indicating the oscillating of temperature peak associated with the bubble oscillation. (*C*) Temperature evolution at several given positions, *A*, *O*, *B* for $\xi = -0.15, 0, 0.25$ mm. (*D*) PDF of the oscillation frequency of the peak temperature at the position of *A* ($\xi = -0.15$ mm) and *B* ($\xi = 0.25$ mm), showing the same oscillation frequency of temperature as that of bubble ($f = 24$ Hz). (*E*) PDF of the oscillation frequency of the peak temperature at the position of center [$f = 48$ Hz at the point *O* ($\xi = 0$ mm)].

(Fig. 2*C*) clearly shows the oscillation with the fluctuation amplitude around 4 K. Accordingly, the oscillation frequency of temperature has a peak at 24 Hz for the point *A* and *B* (Fig. 2*D*), and 48 Hz for the point *O* due to the double frequency at the center (Fig. 2*E*). Evidently, this oscillation frequency of temperature is strongly correlated with the oscillation frequency of bubble (Fig. 1*E*).

Mechanism of the Bubble Oscillation. In order to explore the underlying mechanism of the observed horizontal-oscillation bubble, we proceed to carefully examine the forces subjected to the bubble. Fig. 3*A* shows the temperature distribution and buoyancy-driven natural convection flows inside ethanol under the irradiation of a Gaussian laser beam in the simulation (*SI Appendix*, Supplementary Notes 4 and 5). This natural convection flow is confirmed by particle image velocimetry (PIV) measurement from the side view (*SI Appendix*, Fig. S3). Since the temperature is higher at the center, the thermal Marangoni force (F_M) tends to stabilize or trap the bubble at the center (Fig. 3 *B* and *C*), while the viscous drag force (F_V) tends to sweep the bubble away from the center (Fig. 3*B*). Thus, this competition between the restoring thermal Marangoni force (F_M) and the disturbing viscous drag force (F_V) can cause the spontaneous oscillation.

To quantitatively describe the oscillation criteria, the temperature distribution is assumed to be linearly proportional to the laser intensity distribution in Gaussian form (28), $\Delta T \propto \alpha P e^{-r^2/r_l^2}$, where α is the absorption coefficient of the incident laser intensity in liquids (*SI Appendix*, Table S1). Then, the corresponding thermal Marangoni force F_M can be expressed as follows,

$$F_M = \left(\frac{\partial \gamma}{\partial T}\frac{\partial T}{\partial r}\right)\frac{\pi d^2}{4} \propto \alpha P d^2, \qquad [1]$$

where γ for the surface tension of liquid, and $\partial\gamma/\partial T < 0$ is assumed to be a constant.

Further, the flow velocity v is assumed to be proportional to the position along both r and z direction, e.g. $v \propto U_b rz$, considering the axisymmetric stagnation point flow (32) near the center, where $U_b \propto \sqrt{\alpha P}$ is the typical natural convection flow velocity (28). Then, the viscous drag force can be expressed as follow,

$$F_V = -6\pi\mu v d \propto \sqrt{\alpha P} d^3. \qquad [2]$$

By balancing the thermal Marangoni force F_M (Eq. **1**) and the viscous drag force F_V (Eq. **2**), the scaling relation of the lower bound diameter d_{low} can be obtained,

$$d_{\text{low}} \propto \sqrt{P}, \qquad [3]$$

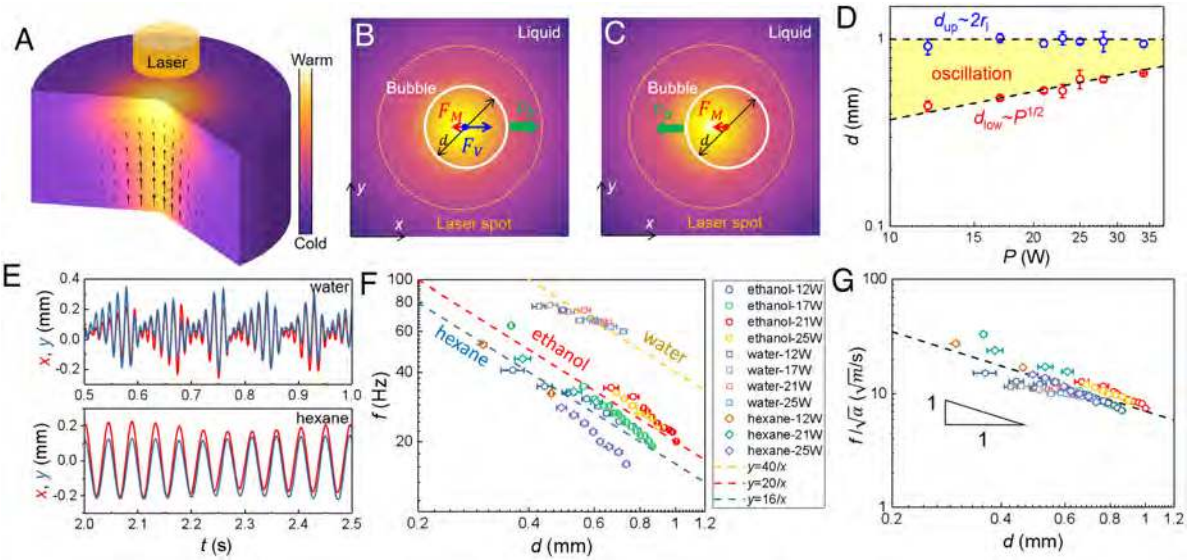

Fig. 3. Mechanism for the horizontal-oscillation bubble. (*A*) Simulation for the temperature distribution and stagnation flow from the side view in the simplified models. (*B* and *C*) Sketches of the viscous driving force (F_V) and the restoring thermal Marangoni force (F_M), which are responsible for the oscillation from the *Top–Down* view. (*D*) The *Lower* (d_{low}) and *Upper* bound diameter (d_{up}) for the oscillating behavior dependent on the laser power P, the dotted lines for theory, and dots for the experiments. (*E*) The horizontal oscillation bubble in other liquids, such as water and hexane, as indicated by the bubble central position (x, y) changing periodically with time t (duration is about 0.5 s) with frequency about 68 and 22 Hz at $P = 25$ W. (*F*) The oscillation frequency of the bubble in three liquids fitted well by scaling of $f \sim d^{-1}$. (*G*) For different liquids, all the data collapsing on a single line of $f/\sqrt{\alpha} \sim d^{-1}$.

which agrees well with the experimental data, as shown in Fig. 3*D*.

When the bubble diameter exceeds a certain value $d > d_{up}$, the bubble turns to float at the center. The upper bound diameter d_{up} seems to be independent of laser power P, and happens to be the diameter of laser beam $d_{up} \approx 2r_l$, highlighting the effect of laser heating on the oscillating motion of bubble.

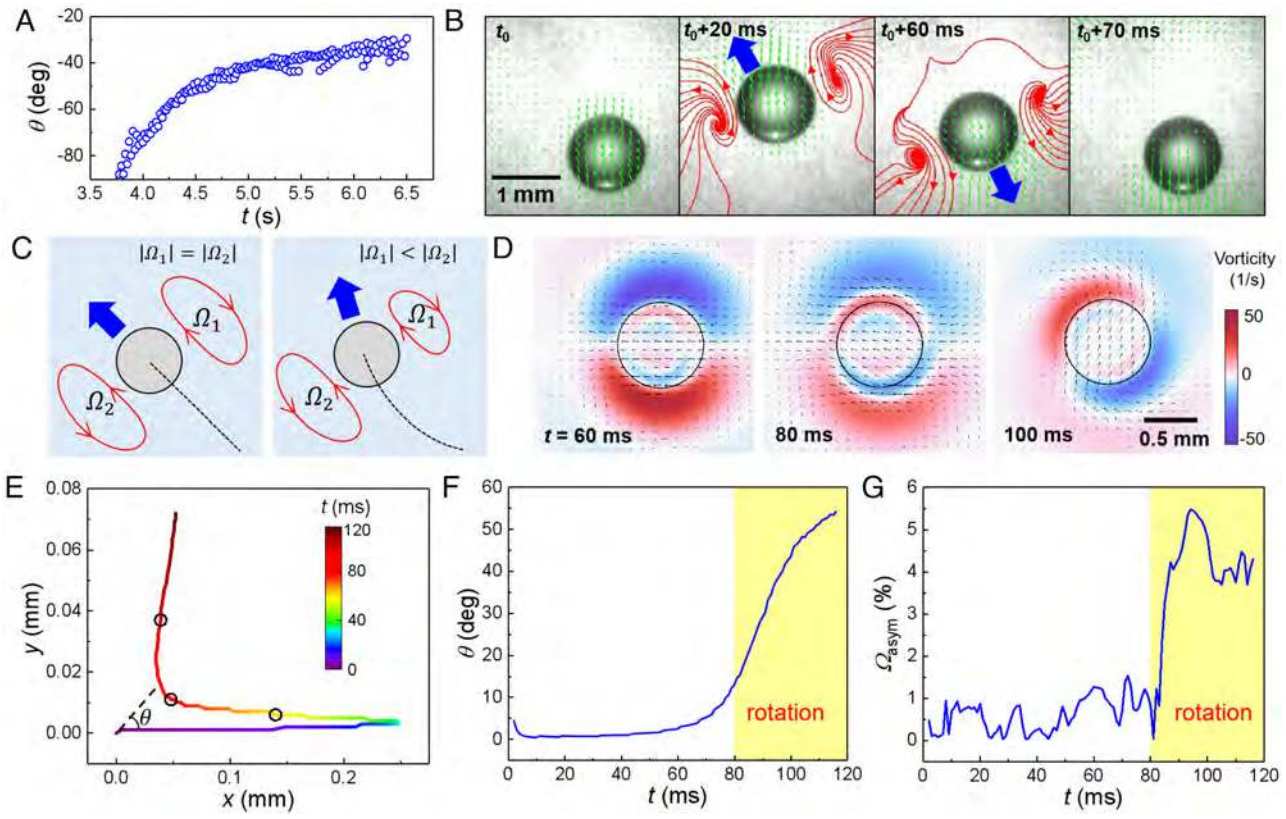

Fig. 4. Rotation of bubble trajectory during oscillations in ethanol. (*A*) The trajectory angle θ (Fig. 1*F*) as a function of time t during bubble oscillation within 3 s. (*B*) PIV-measured flow (green arrow) and streamlines (red lines) during one cycle of bubble oscillation. (*C*) Sketch for the rotation of θ due to the vorticity asymmetry. (*D–G*) Simulation for (*D*) the snapshot showing the flow field around bubble in one typical oscillation cycle and indicating the vorticity distribution around bubble; (*E*) trajectory of the bubble; (*F*) θ and (*G*) vorticity asymmetry (Ω_{asym}) as a function of time.

Scaling Law in Various Liquids. To further validate the observation of the active photothermal bubble, we carry out the experiments by impacting the laser on various liquids, such as water and hexane, and the horizontal-oscillation mode of the bubble is reproduced (Fig. 3*E*). To understand the horizontal-oscillation mode and its oscillation frequency, we adopt the simple "bullet model" and perform scaling analysis to predict the oscillation frequency of bubble by assuming that the disturbing drag force F_V acts as a short impulse force here (27, 28). Then, the oscillation frequency can be expressed as, $f \propto F_M/(m_b U_b)$, where $m_b = 5\pi\rho d^3/12$ considers the added mass of the bubble plus fluid acceleration (33), and the typical velocity of bubble motion is assumed to be the same as the velocity of buoyancy flow U_b.

Then, by incorporating the scaling relation for $U_b \propto \sqrt{\alpha P}$ (28) and $F_M \propto \alpha P d^2$ (Eq. **1**), the scaling dependence of frequency can be derived,

$$f \propto \sqrt{\alpha P}/d. \quad [4]$$

This $f \propto d^{-1}$ scaling relationship between oscillation frequency and bubble size agrees well with the experimental data of ethanol, water, and hexane, as indicated by the dash line in Fig. 3*F*. Furthermore, by considering the absorption coefficient of various liquids, the data $f/\sqrt{\alpha}$ for different liquids collapses well on the same line as well (Fig. 3*G*).

Rotation of Bubble Trajectory. The bubble oscillation trajectory ($\theta \in [-\pi/2, \pi/2]$), as shown in Fig. 1*F*, continuously rotates with time counterclockwise (Fig. 4*A*). To display the flow associated with the rotation of bubble trajectory, PIV is applied to capture flow field during the bubble oscillation (Fig. 4*B* and Movie S4). A vortex pair as indicated by the red streamlines is formed during its oscillation, i.e., one rotates counterclockwise, whereas the other does clockwise.

Generally, the vortex pair during the bubble oscillation likely suffers from the azimuthal perturbations, resulting in the symmetry-broken pair (34–36), as indicated by the sketch in Fig. 4*C*. The asymmetry of the vortex pair is characterized by their vorticity,

$$\Omega_{\text{asym}} = \frac{||\Omega_1| - |\Omega_2||}{|\Omega_1| + |\Omega_2|}, \quad [5]$$

where Ω_1, Ω_2 represent the vorticity of each vortex.

Indeed, the simulation confirms the asymmetry of the vortex pair during the bubble oscillation (Fig. 4*D* and *SI Appendix*, Supplementary Note 5), and the rotation of the bubble trajectory (Fig. 4*E*). By comparing time-dependent θ (Fig. 4*F*) and Ω_{asym} (Fig. 4*G*), the bubble trajectory rotates pronouncedly, as the vorticity asymmetry (Ω_{asym}) becomes significant after $t \geq 80$ ms, indicating the vortex asymmetry responsible for the rotation of bubble trajectory.

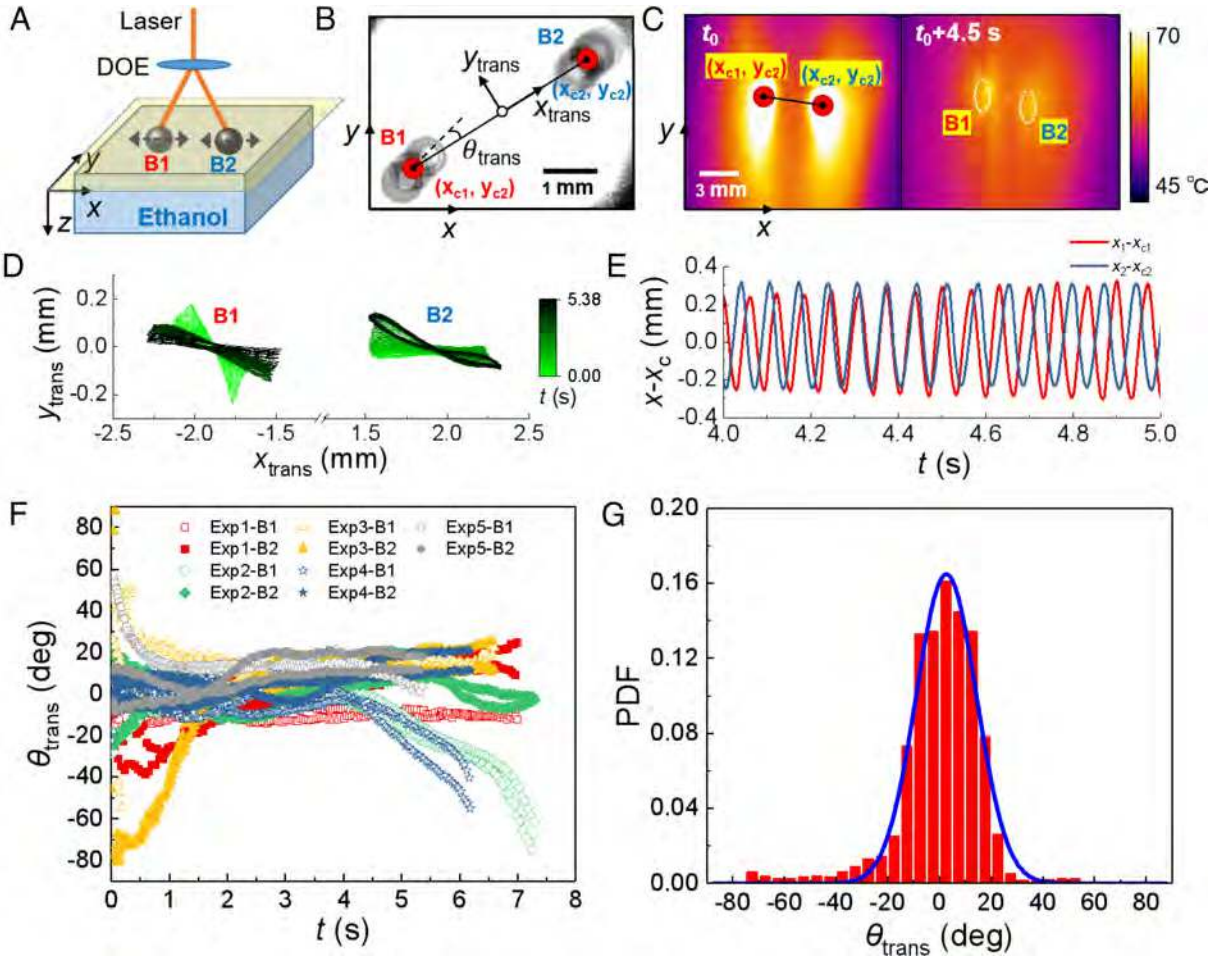

Fig. 5. Double pendulum of two oscillation bubbles. (*A*) Sketch of the oscillation motion for two bubbles by utilizing a DOE to split a single laser beam into double beams. (*B*) The stacked high-speed images showing the oscillation motion of two bubbles in one typical cycle. (*C*) Thermal images showing temperature distribution before (t_0) and after ($t_0 + 4.5$ s) the generation of two bubbles at $P = 42$ W. (*D*) The *Top–Down* view of the two-bubble oscillation trajectory within 5.38 s. (*E*) The trajectory projection along the x_{trans}-axis versus time, indicating the oscillation of two bubbles. (*F*) The time-dependent angle θ_{trans} of two bubbles in five sets of data. (*G*) PDF of the oscillation angle θ_{trans} for all data in (*F*), and the blue line for the fitting of Gaussian distribution.

The "Double Pendulum" of Oscillation Bubbles. Since the horizontal-oscillation bubble is similar to the periodic motion of an oscillation pendulum, in order to mimic the double pendulum (37, 38), two coupled oscillation bubbles are investigated. A single laser beam with Gaussian intensity distribution is split by a diffractive optical element (DOE, DS-237-I-N-A, Holoor) into two beams, which impacts on ethanol. Once the laser power exceeds 25 W (almost twice of the threshold value for the single laser beam case by considering the 94% power transmission efficiency of the DOE), two photothermal bubbles are produced (Fig. 5*A*). The center of two laser beams at the air–liquid interface is carefully adjusted to be close enough around 4 mm, so that the coupling effect of two bubbles can be surveyed.

Fig. 5*B* shows the stacked high-speed images of the two coupled bubbles within one oscillation period (Movie S5). This favorable coupled oscillation direction seems to be along the line of the two laser spots and is reasonably consistent with the symmetry breaking of the thermal distribution (Fig. 5*C*). The two bubbles are separated by a cold temperature region in the middle of the two beam spots, and the temperature asymmetry is more pronounced in the direction of the line connecting the two spots (x_{trans}-axis) (Movie S6).

To quantitatively characterize the dynamics of two bubbles, a coordinate transformation is applied, and the (x, y) coordinate system is transformed to the $(x_{\text{trans}}, y_{\text{trans}})$ coordinate system, and the rotation angle θ_{trans} is defined as the angle between the bubble oscillation axis and the x_{trans}-axis. Then Fig. 5*D* presents the oscillation trajectory of the two bubbles, and Fig. 5*E* indicates the periodic motion of these two bubbles. Due to many complicated factors associated with the oscillation frequency, including temperature distribution from heat transfer, bubble size and growth, and transient viscous flows, their individual oscillation frequency can be different. Here, their peak frequency is $f_1 = 15.0$ Hz, $f_2 = 14.0$ Hz, and the relative frequency difference is $\Delta f/\bar{f} = |f_1 - f_2| / [(f_1 + f_2)/2] = 6.8\%$.

By analyzing the time-dependent oscillation angle θ_{trans} for several pairs of oscillating bubbles (Fig. 5*F*), the PDF of the oscillation angle (Fig. 5*G*) implies the oscillation angle of the two bubbles has a Gaussian distribution with a center value of zero degrees, suggesting that the oscillating directions of bubbles tend to be along the laser spot center-line.

Methods

Experimental Setup. The experimental setup is shown in *SI Appendix*, Fig. S1. The liquid was contained in a quartz glass cuvette (20 × 20 × 10 mm) covered with a glass slide (sapphire, which is optically transparent for the irradiating laser). An infrared laser source at 980 nm wavelength was slightly focused on the liquid sample transmitted through the cover glass from the top side. Bubble was illuminated from side and below respectively with two xenon lamps, and its dynamics was captured by two synchronized fast-speed cameras (Phantom V611 and C110). The data extracted from high-speed images, e.g. the bubble diameter and position, are obtained by using ImageJ software with an analytical error of about 2 pixels. The temperature evolution of local ethanol during the laser irradiating was acquired by an infrared thermal camera (FLIR A6750sc, operating in 1 to 5 μm range, accuracy 1 °C). Due to the high transmissivity @185 to 5,000 nm of the sapphire cover glass, the infrared light can optically penetrate through the sapphire into the thermal camera, thus ensuring the accurate temperature measurements.

Numerical Simulation. To simulate the temperature and flow field induced by laser heating, the Navier–Stokes equation and heat transfer equation are solved in axisymmetric cylindrical coordinate (r, θ, z), including the volumetric heat source and the gravity. To simulate the bubble oscillation and trajectory rotation, the Navier–Stokes equation is solved in Cartesian coordinate (x, y), using the phase field method to track the liquid–gas interface. The variation of liquid properties with temperature, such as density and surface tension, is simplified to linear functions. All the models are solved by COMSOL Multiphysics.

Data, Materials, and Software Availability. All study data are included in the article and/or supporting information.

ACKNOWLEDGMENTS. We are thankful for the fruitful discussions with Professor K. L. Chong. M.H. acknowledges the Shanghai Science and Technology Program under project No. 23ZR1403800; F.W. acknowledges Shuimu Tsinghua Scholar Program under Grant No. 2023SM038; and D.D. acknowledges the funding by the National Program in China and the Startup in Fudan University.

1. M. C. Marchetti et al., Hydrodynamics of soft active matter. *Rev. Mod. Phys.* **85**, 1143 (2013).
2. C. Bechinger *et al.*, Active particles in complex and crowded environments. *Rev. Mod. Phys.* **88**, 045006 (2016).
3. E. Lauga, T. R. Powers, The hydrodynamics of swimming microorganisms. *Rep. Prog. Phys.* **72**, 096601 (2009).
4. P. H. Colberg, S. Y. Reigh, B. Robertson, R. Kapral, Chemistry in motion: Tiny synthetic motors. *Acc. Chem. Res.* **47**, 12 3504 (2014).
5. T. E. Mallouk, A. Sen, Powering nanorobots. *Sci. Am.* **300**, 72 (2009).
6. Y. Feng, M. An, Y. Liu, M. T. Sarwar, H. M. Yang, Advances in chemically powered micro/nanorobots for biological applications: A Review. *Adv. Funct. Mater.* **33**, 2209883 (2023).
7. R. Dreyfus et al., Microscopic artificial swimmers. *Nature* **437**, 862 (2005).
8. L. Zhang *et al.*, Artificial bacterial flagella: Fabrication and magnetic control. *Appl. Phys. Lett.* **94**, 064107 (2009).
9. M. Mijalkov, G. Volpe, Sorting of chiral microswimmers. *Soft Matter* **9**, 6376 (2013).
10. B. Liebchen, H. Lowen, Synthetic chemotaxis and collective behavior in active matter. *Acc. Chem. Res.* **51**, 2982 (2018).
11. R. F. Ismagilov, A. Schwartz, N. Bowden, G. M. Whitesides, Autonomous movement and self-assembly. *Angew. Chem. Int. Ed.* **41**, 652 (2002).
12. W. F. Paxton *et al.*, Catalytic nanomotors: Autonomous movement of striped nanorods. *J. Am. Chem. Soc.* **126**, 13424 (2004).
13. J. L. Moran, J. D. Posner, Phoretic self-propulsion. *Annu. Rev. Fluid Mech.* **49**, 511 (2017).
14. A. Zöttl, H. Stark, Modeling active colloids: From active brownian particles to hydrodynamic and chemical fields. *Annu. Rev. Condens. Matter Phys.* **14**, 109 (2023).
15. S. Michelin, Self-propulsion of chemically active droplets. *Annu. Rev. Fluid Mech.* **55**, 77 (2023).
16. S. Herminghaus et al., Interfacial mechanisms in active emulsions. *Soft Matter* **10**, 7008 (2014).
17. C. C. Maass, C. Krüger, S. Herminghaus, C. Bahr, Swimming droplets. *Annu. Rev. Condens. Matter Phys.* **7**, 171 (2016).
18. S. J. Kim, Z. Kos, E. Um, J. Jeong, Symmetrically pulsating bubbles swim in an anisotropic fluid by nematodynamics. *Nat. Commun.* **15**, 1220 (2024).
19. E. Jambon-Puillet *et al.*, Phase-separated droplets swim to their dissolution. *Nat. Commun.* **15**, 3919 (2024).
20. M. Kumar, A. Murali, A. G. Subramaniam, R. Singh, S. Thutupalli, Emergent dynamics due to chemo-hydrodynamic self-interactions in active polymers. *Nat. Commun.* **15**, 4903 (2024).
21. D. Baigl, Photo-actuation of liquids for light-driven microfluidics: State of the art and perspectives. *Lab Chip* **12**, 3637 (2012).
22. K. Dietrich, N. Jaensson, I. Buttinoni, G. Volpe, L. Isa, Microscale Marangoni surfers. *Phys. Rev. Lett.* **125**, 098001 (2020).
23. C. Maggi, F. Saglimbeni, M. Dipalo, F. D. Angelis, R. D. Leonardo, Micromotors with asymmetric shape that efficiently convert light into work by thermocapillary effects. *Nat. Commun.* **6**, 7855 (2015).
24. J. Q. Song, J. H. Zhang, S. K. Mani, A. Sen, Droplet navigation by photothermal pumping in an optofluidic system. *Langmuir* **38**, 11486 (2022).
25. X. L. Li et al., Laser controlled manipulation of microbubbles on a surface with silica-coated gold nanoparticle array. *Small* **19**, 2302939 (2023).
26. F. L. Wang *et al.*, Plasmonic bubbles: From fundamentals to applications. *Adv. Funct. Mater.* **34**, 2403606 (2024).
27. B. L. Zeng *et al.*, Periodic bouncing of a plasmonic bubble in a binary liquid by competing solutal and thermal marangoni forces. *Proc. Natl. Acad. Sci. U.S.A.* **118**, e2103215118 (2021).
28. M. Hu *et al.*, Near-infrared-laser-navigated dancing bubble within water via a thermally conductive interface. *Nat. Commun.* **13**, 5749 (2022).
29. Y. T. Li *et al.*, Oil-on-water droplets faceted and stabilized by vortex halos in the subphase. *Proc. Natl. Acad. Sci. U.S.A.* **120**, e2214657120 (2023).
30. S. Kedenburg, M. Vieweg, T. Gissibl, H. Giessen, Linear refractive index and absorption measurements of nonlinear optical liquids in the visible and near-infrared spectral region. *Opt. Mater. Express* **2**, 1588 (2012).
31. Y. L. Wang *et al.*, Vapor and gas-bubble growth dynamics around laser-irradiated, water-immersed plasmonic nanoparticles. *ACS Nano* **11**, 2045 (2017).
32. H. Schlichting, K. Gersten, *Boundary-Layer Theory* (Springer, 2016).

33. R. Toegel, S. Luther, D. Lohse, Viscosity destabilizes sonoluminescing bubbles. *Phys. Rev. Lett.* **96**, 114301 (2006).
34. G. Koleski, A. Vilquin, J. C. Loudet, T. Bickel, B. Pouligny, Azimuthal instability of the radial thermocapillary flow around a hot bead trapped at the water-air interface. *Phys. Fluids* **32**, 092108 (2020).
35. K. Drescher, R. E. Goldstein, N. Michel, M. Polin, I. Tuval, Direct measurement of the flow field around swimming microorganisms. *Phys. Rev. Lett.* **105**, 168101 (2010).
36. J. S. Guasto, K. A. Johnson, J. P. Gollub, Oscillatory flows induced by microorganisms swimming in two dimensions. *Phys. Rev. Lett.* **105**, 168102 (2010).
37. A. W. Hauser, S. Sundaram, R. C. Hayward, Photothermocapillary oscillators. *Phys. Rev. Lett.* **121**, 158001 (2018).
38. H. Kim *et al.*, Coupled oscillation and spinning of photothermal particles in marangoni optical traps. *Proc. Natl. Acad. Sci. U.S.A.* **118**, e2024581118 (2021).